A variant transfer matrix method suitable for transport through multi-probe systems

2007 Nanotechnology 18 435402

(http://iopscience.iop.org/0957-4484/18/43/435402)

IOP PUBLISHING NANOTECHNOLOGY
Nanotechnology **18** (2007) 435402 (6pp) doi:10.1088/0957-4484/18/43/435402

A variant transfer matrix method suitable for transport through multi-probe systems

Zhenhua Qiao and Jian Wang

Department of Physics and the Center of Theoretical and Computational Physics,
The University of Hong Kong, Hong Kong, People's Republic of China

Received 21 May 2007, in final form 8 September 2007
Published 4 October 2007
Online at stacks.iop.org/Nano/18/435402

Abstract
We have developed a variant transfer matrix method that is suitable for transport through multi-probe systems. Using this method, we have numerically studied the quantum spin Hall effect (QSHE) on 2D graphene with both intrinsic (V_{so}) and Rashba (V_r) spin–orbit (SO) couplings. The integer QSHE arises in the presence of intrinsic SO interaction and is gradually destroyed by the Rashba SO interaction and disorder fluctuation. We have numerically determined the phase boundaries separating integer QSHE and spin Hall liquid. We have found that when $V_{so} \geqslant 0.2t$ with t the hopping constant the energy gap needed for the integer QSHE is the largest satisfying $|E| < t$. For smaller V_{so} the energy gap decreases linearly. In the presence of Rashba SO interaction or disorders, the energy gap diminishes. With Rashba SO interaction the integer QSHE is robust at the largest energy within the energy gap while at the smallest energy within the energy gap the integer QSHE is insensitive to the disorder.

(Some figures in this article are in colour only in the electronic version)

1. Introduction

Graphene is a two-dimensional honeycomb lattice of a single-atomic carbon layer and has a special band structure. With more and more experimental discoveries and theoretical predictions [1–6], there is currently intense interest in electronic properties of the graphene sheet. In particular, the spin Hall effect (SHE) has the potential to provide a purely electrical means to control the spin of electrons in the absence of non-ferromagnetic materials and magnetic field [7]. This is because the spin–orbit interaction in the graphene exerts a torque on the spin of the electron, whose precessing leads to a spin polarized current. In a four-probe device, this spin polarized current can lead to a pure spin current without accompanying charge current [8]. It has been proposed by Haldane [9] that a quantum Hall effect may exist in the absence of magnetic field. Similarly, an integer quantum spin Hall effect can exist on a honeycomb lattice when the intrinsic spin–orbit interaction is present [7, 10]. In the presence of disorder the charge conductance of mesoscopic conductors shows universal features with a universal conductance fluctuation [11] and the spin Hall conductance also fluctuates with a universal value [12] in the presence of spin–orbit interaction. The presence of disorder can also destroy the integer quantum spin Hall effect and quantum Hall effect [13] for a graphene system with intrinsic spin–orbit interaction [7]. Hence it is of interest to map out the phase diagram for the integer quantum spin Hall effect. In this paper, we investigate the disorder effect on the spin Hall current for a four-probe graphene system in the presence of intrinsic and/or Rashba SO interactions, denoted as V_{so} and V_r, respectively. For such a system, the conventional transfer matrix method can not be used. So the direct matrix inversion method must be used to obtain the Green function that is needed for the transport properties. As a result, the simulation of a multi-probe system using the direct method is very calculationally demanding.

In this paper, we develop an algorithm based on the idea of the transfer matrix that is much faster than the direct method. As an application, we have numerically mapped out the phase diagram for a two-dimensional honeycomb lattice in the presence of the intrinsic and/or Rashba SO interactions and disorders. When turning on the Rashba SO interaction, we found that the energy gap needed for the IQSHE is $|E| < t$ for $V_{so} \geqslant 0.2t$ and decreases linearly when $V_{so} < 0.2t$. In the presence of Rashba SO interaction, the phase diagram (E, V_r) is asymmetric about the Fermi energy. The IQSHE is more difficult to destroy at the largest energy of the energy gap. In the presence of disorder, the phase diagram (E, W) is again

asymmetric about the Fermi energy but it is the smallest energy of the energy gap that is robust against the disorder fluctuation.

2. Theoretical formalism

In the tight-binding representation, the Hamiltonian for the 2D honeycomb lattice of the graphene structure can be written as [7, 9]

$$H = -t\sum_{<ij>} c_i^\dagger c_j + \frac{2\mathrm{i}}{\sqrt{3}}V_{\mathrm{so}}\sum_{\ll ij\gg} c_i^\dagger \sigma\cdot(\mathbf{d}_{kj}\times\mathbf{d}_{ik})c_j + \mathrm{i}V_{\mathrm{r}}\sum_{<ij>} c_i^\dagger \hat{\mathbf{e}}_z\cdot(\sigma\times\mathbf{d}_{ij})c_j + \sum_i \epsilon_i c_i^\dagger c_i \quad (1)$$

where $c_i^\dagger$ (c_i) is the electron creation (annihilation) operator and the σ are Pauli matrices. The first term is due to the nearest hopping. The second term is the intrinsic spin–orbit interaction that involves the next nearest sites. Here i and j are two next nearest neighbor sites, k is the common nearest neighbor of i and j, and $\mathbf{d}_{ik}$ describes a vector pointing from k to i. The third term is due to the Rashba spin–orbit coupling. The last term is the on-site energy, where ϵ_i is a random on-site potential uniformly distributed in the interval $[-W/2, W/2]$. In this Hamiltonian, we have set the lattice constant to be unity.

We consider a four-probe device as shown schematically in figure 1(a). The four probes are exactly the extension from the central scattering region; i.e., the probes are graphene ribbons. The number of sites in the scattering region is denoted as $N = n_x \times n_y$, where there are $n_x = 8\times n+1$ sites on $n_y = 4\times n$ chains (figure 1(a) shows the cell for $n = 1$)[1]. We apply external bias voltages V_i with $i = 1, 2, 3, 4$ at the four different probes as $V_i = (v/2, 0, -v/2, 0)$. In the presence of Rashba SO interaction, the spin is not a good quantum number. As a result, the spin current is not conserved using the conventional definition. Hence we switch off the Rashba SO interaction in the second and fourth probes. Similar to the setup of [7], our setup can generate an integer quantum spin Hall effect. The difference between the setup of [7] and ours is that the lead in [7] is a square lattice without SO interactions while our lead is still a honeycomb lattice with SO interactions except that the Rashba SO interaction has been switched off in leads 2 and 4. The use of the square lattice as a lead has two consequences. It provides additional interfacial scattering between the scattering region and the lead due to the lattice mismatch and the mismatch in SO interactions. In addition, the dimension of the self-energy matrix for the square lattice lead with SO interaction is much smaller. The spin Hall conductance G_{sH} can be calculated from the multi-probe Landauer–Buttiker formula [8, 12]:

$$G_{\mathrm{sH}} = (e/8\pi)[(T_{2\uparrow,1} - T_{2\downarrow,1}) - (T_{2\uparrow,3} - T_{2\downarrow,3})] \quad (2)$$

where the transmission coefficient is given by $T_{2\sigma,1} = \mathrm{Tr}(\Gamma_{2\sigma}G^{\mathrm{r}}\Gamma_1 G^{\mathrm{a}})$ with $G^{\mathrm{r,a}}$ being the retarded and advanced Green functions of the central disordered region, which can be evaluated numerically. The quantities $\Gamma_{i\sigma}$ are the linewidth functions describing coupling of the probes and the scattering region and are obtained by calculating self-energies Σ^{r} due to the semi-infinite leads using a transfer matrix method [14]. In the following, our numerical data are mainly on a system with $n = 8$ or 32×65 sites in the system. To fix units, throughout this paper, we define the Fermi energy E, disorder strength W, intrinsic spin–orbit coupling V_{so} and Rashba spin–orbit coupling V_{r} in terms of the hopping energy t.

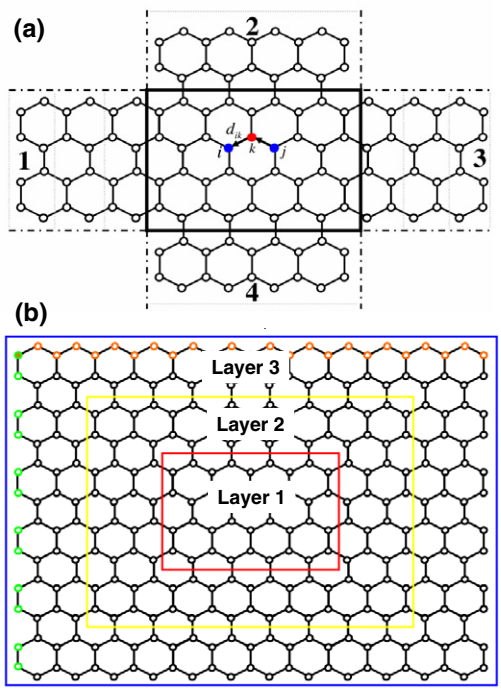

Figure 1. Schematic plot of the four-terminal mesoscopic sample where the intrinsic SO interaction exists in the center scattering region and leads 1 and 3 and the Rashba SO only exists in the center part and leads 1 and 3, when the spin Hall conductance is measured through leads 2 and 4.

For the four-probe device, the conventional transfer matrix that is suitable for two-probe devices can no longer be used. Below, we provide a modified transfer matrix method for the four-probe device. Note that the self-energy Σ^{r} is a matrix with non-zero elements at those positions corresponding to the interface sites between a lead and the scattering region[2]. Because evaluating the Green function G^{r} corresponds to the inversion of a matrix, a reasonable numbering scheme for the lattice sites can minimize the bandwidth of the matrix and thus reduce the cost of numerical computation. For example, to obtain the narrowest bandwidth for our system we partition the system into layers shown in figure 1(b) so that there is no coupling between the next nearest layers. We then label each site layer by layer from the center of the system (see figure 1(a)). As a result, the matrix $E - H - \Sigma^{\mathrm{r}}$ becomes a block tri-diagonal matrix:

$$E - H - \Sigma^{\mathrm{r}} = \begin{pmatrix} A_1 & C_1 & . & . & . & . \\ B_2 & A_2 & C_2 & . & . & . \\ . & . & . & . & . & . \\ . & . & . & . & . & . \\ . & . & . & . & A_{m-1} & C_{m-1} \\ . & . & . & . & B_m & A_m \end{pmatrix}$$

[1] Here we follow the same labeling scheme as [7].

[2] In the presence of intrinsic SO interaction the lead couples to the sites on the two layers in the interfaces.

where A_n is a $(128n - 56) \times (128n - 56)$ matrix, C_n is a $(128n - 56) \times (128n + 72)$ matrix, and B_n is a $(128n - 56) \times (128n - 184)$ matrix. Here $n = 1$ corresponds to the innermost layer and $n = m$ is for the outermost layer. A direct inversion of this block tri-diagonal matrix is already faster than the other labeling schemes. However, if we are interested in the transmission coefficient, it is not necessary to invert the whole matrix. This is because the self-energies of the leads are coupled only to A_m of the outermost layers; from Landauer–Buttiker's formula it is enough to calculate the Green function G^{r}_{mm} which satisfies the following Equation:

$$(E - H - \Sigma^{\mathrm{r}}) \begin{pmatrix} G^{\mathrm{r}}_{1m} \\ G^{\mathrm{r}}_{2m} \\ . \\ . \\ G^{\mathrm{r}}_{m-1m} \\ G^{\mathrm{r}}_{mm} \end{pmatrix} = \begin{pmatrix} 0 \\ 0 \\ . \\ . \\ 0 \\ I_m \end{pmatrix}$$

where I_m is a unit matrix of dimension m. In general, the solution X_i of the following equation with block tri-diagonal matrix can be easily obtained.

$$\begin{pmatrix} A_1 & C_1 & . & . & . & . \\ B_2 & A_2 & C_2 & . & . & . \\ . & . & . & . & . & . \\ . & . & . & . & . & . \\ . & . & . & . & A_{m-1} & C_{m-1} \\ . & . & . & . & B_m & A_m \end{pmatrix} \begin{pmatrix} X_1 \\ X_2 \\ . \\ . \\ X_{m-1} \\ X_m \end{pmatrix} = \begin{pmatrix} R_1 \\ R_2 \\ . \\ . \\ R_{m-1} \\ R_m \end{pmatrix}.$$

From the first row

$$A_1 X_1 + C_1 X_2 = R_1,$$

we have

$$X_1 + A_1^{-1} C_1 X_2 = A_1^{-1} R_1.$$

From the second row,

$$B_2 X_1 + A_2 X_2 + C_2 X_3 = R_2,$$

eliminating X_1, we have

$$(A_2 - B_2 A_1^{-1} C_1) X_2 + C_2 X_3 = R_2 - B_2 A_1^{-1} R_1.$$

This equation can be written as

$$F_2 X_2 + C_2 X_3 = D_2,$$

where

$$F_2 = A_2 - B_2 A_1^{-1} C_1,\ D_2 = R_2 - B_2 A_1^{-1} R_1.$$

From the third row,

$$B_3 X_2 + A_3 X_3 + C_3 X_4 = R_3,$$

eliminating X_2, we have

$$F_3 X_3 + C_3 X_4 = D_3,$$

where

$$F_3 = A_3 - B_3 F_2^{-1} C_2,\ D_3 = R_3 - B_3 F_2^{-1} D_2.$$

Therefore, we have the following recursion relation:

$$\begin{array}{lll} F_1 = & A_1, & \text{initial} \\ F_i = & A_i - B_i F_{i-1}^{-1} C_{i-1}, & i = 2, 3, \ldots, m \\ D_1 = & R_1, & \text{initial} \\ D_i = & R_i - B_i F_{i-1}^{-1} D_{i-1}, & i = 2, 3, \ldots, m. \end{array}$$

Finally, we have

$$\begin{pmatrix} F_1 & C_1 & . & . & . & . \\ . & F_2 & C_2 & . & . & . \\ . & . & . & . & . & . \\ . & . & . & . & . & . \\ . & . & . & . & F_{m-1} & C_{m-1} \\ . & . & . & . & . & F_m \end{pmatrix} \begin{pmatrix} X_1 \\ X_2 \\ . \\ . \\ X_{m-1} \\ X_m \end{pmatrix} = \begin{pmatrix} D_1 \\ D_2 \\ . \\ . \\ D_{m-1} \\ D_m \end{pmatrix}.$$

From the last row, we can solve for X_m:

$$X_m = F_m^{-1} D_m.$$

We can cancel X_m in the last but one equation

$$X_{m-1} = F_{m-1}^{-1} (D_{m-1} - C_{m-1} X_m).$$

In our case, $X_i = G^{\mathrm{r}}_{im}$ and $R_i = \delta_{im} I_m$ and we are only interested in the solution G_{mm}. Hence we have the solution

$$G^{\mathrm{r}}_{mm} = F_m^{-1}$$

where

$$\begin{array}{ll} F_1 = & A_1, \\ F_i = & A_i - B_i F_{i-1}^{-1} C_{i-1}, \quad i = 2, 3, \ldots, m. \end{array}$$

To test the speed of this algorithm, we have calculated the spin Hall conductance for the four-probe graphene system with different system size labeled by n on a Matlab platform. The calculation is done at a fixed energy and for 1000 random configurations. The cpu times are listed in table 1, where the speed of direct matrix inversion and the algorithm just described are compared. We see that the speedup factor increases as the system size increases. For instance, for $n = 8$, which corresponds to 2080 sites (amounting to a 4016×4016 matrix) in the scattering region, a factor of 100 is gained in speed. We note that in the presence of intrinsic SO interaction the coupling involves next nearest neighbor interaction. This is the major factor that slows down our algorithm. As shown in table 1, for a square lattice without intrinsic SO interaction but with Rashba SO interaction, the speedup factor is around 200 for a 40×40 system (matrix dimension 3200). The

Table 1. The cpu times for different system sizes using different methods are calculated at a fixed Fermi energy for 1000 random configurations.

A four-probe graphene			A four-probe square lattice		
System size n	Direct method (s)	Our method (s)	System size L	Direct method (s)	Our method (s)
6	14 803	383	30	5 102	53
7	31 491	606	40	29 337	152
8	104 275	958	50	89 917	309

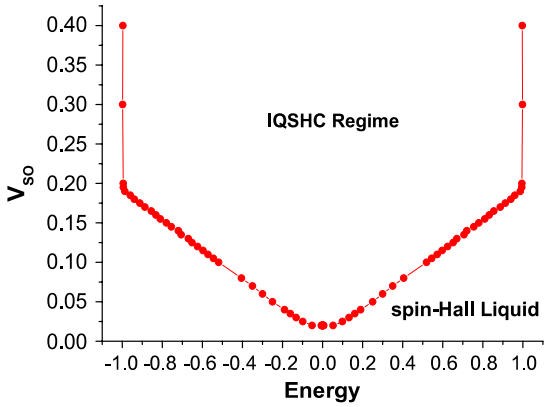

Figure 2. Phase diagram of IQSHC on the (E, V_{so}) plane for $W = 0$ and $V_r = 0$. The curve separates the IQSHC regime and the spin Hall liquid regime.

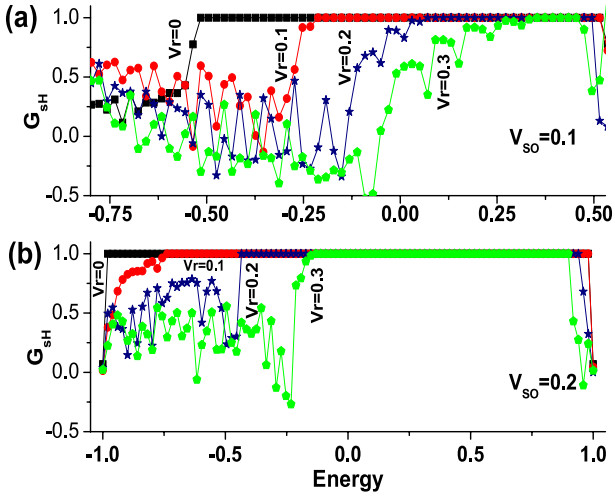

Figure 3. Spin Hall conductance versus electron Fermi energy for $V_r = 0, 0.1, 0.2, 0.3$ on the $N = 32 \times 65$ sample. (a) For $W = 0$ and $V_{so} = 0.1$; (b) for $W = 0$ and $V_{so} = 0.2$.

new algorithm is particularly useful when a large number of disordered samples and different sample sizes are needed for the calculation of the conductance fluctuation and its scaling with size. Finally, we wish to mention that this algorithm also applies to multi-probe systems such as six-probe systems.

3. Numerical results

It has been shown that in the presence of disorder or Rashba SO interaction the QSHE may be destroyed [7]. As an application of our algorithm, we study the phase boundary between regimes of the integer QSHE regime and the QSH liquid in the presence of disorder. For this purpose, we set a criterion for the QSH; i.e., if $G_{sH} \geqslant 0.999$ we say it reaches an integer quantum spin Hall plateau (IQSH). Since the integer QSHE is due to the presence of intrinsic SOI, we first study the phase diagram of a clean sample in the absence of Rashba SOI, i.e. the two-component Haldane's model [9]. For this model, there is an energy gap within which the IQSH effect exists. Figure 2 depicts the phase diagram in the (E, V_{so}) plane with a curve separating the integer QSHE and SHE liquid. We see that the phase diagram is symmetric about the Fermi energy E and the integer QSHE exists only for energy $E < 1$ that corresponds to the energy gap. Figure 2 shows that the energy gap depends on the strength of intrinsic SO interaction. When $V_{so} \geqslant 0.2$ the energy gap is the largest between $E = [-1, 1]$, while for $V_{so} < 0.2$ the energy gap gradually diminishes to zero in a linear fashion. Our numerical data show that for $V_{so} < 0.025$ the IQSHE disappears (see figure 2). Between $V_{so} = [0.025, 0.18]$ the phase boundary is a linear curve. When $V_{so} > 0.20$, the phase boundary becomes a sharp vertical line.

For Haldane's model, σ_z is a good quantum number. However, in the presence of Rashba SOI the spin experiences a spin torque while traversing the system. This can destroy the IQSHE at large enough Rashba SOI strength V_r. In figure 3, we show the spin Hall conductance G_{sH} versus Fermi energy at different V_r when $V_{so} = 0.1, 0.2$. In figure 3(a) we see that when $V_r = 0$ the spin Hall conductance is quantized between $E = -0.52$ and $+0.52$. As V_r increases to 0.1, the energy gap decreases to -0.22 and 0.51. Upon further increasing V_r to 0.2 and 0.3, the gaps shrink to, respectively, [0.06, 0.50] and [0.34, 0.46]. In [7] the IQSHE is completely destroyed when $V_r = 0.3$, which is different from our result. The difference is due to the lead used in [7] that causes additional scattering. The larger the intrinsic SO interaction strength V_{so}, the more difficult it is to destroy the integer QSHE, as can be seen from figure 3(b).

In the presence of Rashba SO interaction the phase diagram in the (E, V_r) plane at different intrinsic SO interaction strengths is shown in figure 4. We see that the phase diagram is asymmetric about the Fermi energy and it is more difficult to destroy the integer QSHE for largest positive energies within the energy gap, e.g. near $E = 0.51$ when $V_{so} = 0.1$. Similar to figure 2, we see that when $V_{so} > 0.2$ integer QSHE can exist for all energies as long as $|E| < 1$. Roughly speaking, the energy gap decreases linearly with increasing Rashba SOI and there is a threshold V_r beyond which the integer QSHE disappears. For instance, when $V_r > 0.3$ and $V_{so} = 0.1$, the integer QSHE is destroyed.

From the above analysis, we see that $V_{so} = 0.2$ is an important point separating two different behaviors in (E, V_{so})

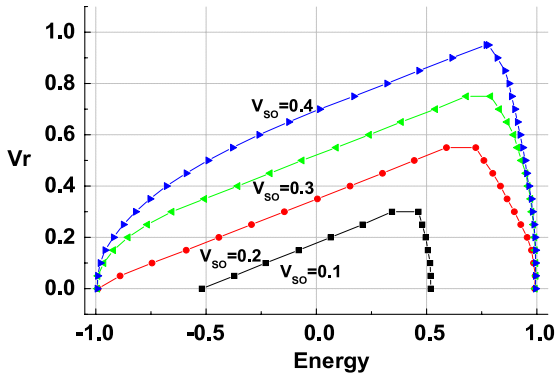

Figure 4. Phase diagram for integer quantum spin Hall conductance on the (E, V_r) plane. Squares, circles, left triangles and right triangles are for $V_{so} = 0.1$, 0.2, 0.3 and 0.4, respectively. The areas encircled by the curves and the $V_r = 0$ line are the integer quantum spin Hall conductance regimes for different intrinsic SOI.

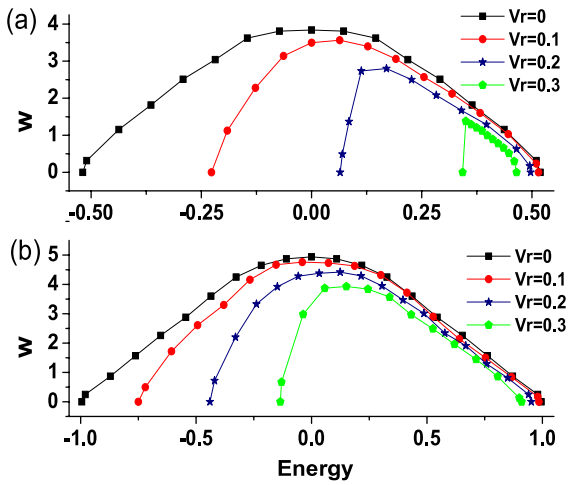

Figure 5. Phase diagram of IQSHC on the (E, W) plane for different Rashba SO couplings in the presence of (a) $V_{so} = 0.1$ and (b)$V_{so} = 0.2$. Squares, circles, stars and rhombuses are for $V_r = 0$, 0.1, 0.2, 0.3. The areas encircled by the curves and the $W = 0$ line are the IQSHC regimes for different Rashba SOI.

and (E, V_r) phase diagrams. Now we examine the effect of disorder on the QSHE. Figure 5 shows the phase diagram of integer QSHE on (E, W) at two typical intrinsic SO interaction strengths $V_{so} = 0.1$ and $V_{so} = 0.2$. The phase diagrams are asymmetric about the Fermi energy. Generally speaking, the larger the Rashba SO interaction strength V_r, the smaller the energy gap needed for integer QSHE. We already see from figure 4 that the integer QSHE is more robust against Rashba SO interaction strength V_r at positive Fermi energy within the energy gap. In contrast, it is small Fermi energies within the energy gap that are stable against the disorder fluctuation, especially for large Rashba SO interaction strength. In addition, the phase boundary at positive Fermi energy is not very sensitive to the variation of Rashba SO interaction strength. The larger the intrinsic SO interaction, the larger the disorder strength W_c needed to destroy the integer QSHE. In figure 6, we estimate this critical disorder strength W_c and plot it versus V_{so} for $E = 0.01$ and $V_r = 0$.

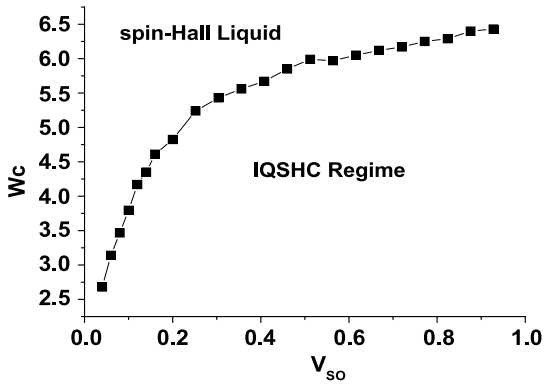

Figure 6. The critical disorder strength versus intrinsic SO coupling V_{so}. The corresponding Fermi energy is $E = 0.01$ and $V_r = 0$. The spin Hall conductance in the regime encircled by the curve and the Rashba SOI axis is well quantized.

If we replace the Rashba SO interaction by the Dresselhaus SO interaction, we have numerically confirmed that the phase diagram of IQSHC in the (E, W) plane is the same if we change E for $-E$.

In summary, we have developed a variant transfer matrix method that is suitable for multi-probe systems. With this algorithm, the speed gained is a factor of 100 for a system of 2080 sites with the next nearest SO interaction on a honeycomb lattice. For the square lattice with Rashba SO interaction, the speed gained is around 200 for a 40×40 system. Using this algorithm, we have studied the phase diagrams of the graphene with intrinsic and Rashba SO interaction in the presence of disorder.

Acknowledgments

This work was financially supported by RGC grant HKU 7048/06P from the government of the SAR of Hong Kong and LuXin Energy Group. The Computer Center of The University of Hong Kong is gratefully acknowledged for the high-performance computing facility.

References

[1] Novoselov K S, Geim A K, Morozov S V, Jiang D, Katsnelson M I, Grigorieva I V, Dubonos S V and Firsov A A 2005 *Nature* **438** 197
[2] Zhang Y, Tan Y W, Störmer H L and Kim P 2005 *Nature* **438** 201
[3] Zhang Y, Jiang J, Small J P, Purewal M S, Tan Y W, Fazlollahi M and Chudow J D 2006 *Phys. Rev. Lett.* **96** 136806
[4] Gusynin V P and Sharapov S G 2005 *Phys. Rev. Lett.* **95** 146081
[5] Peres N M R, Castro Neto A H and Guinea F 2006 *Phys. Rev.* B **73** 195411
[6] Son Y W, Cohen M L and Louie S G 2006 *Preprint* cond-mat/0611600
[7] Sheng L, Sheng D N, Ting C S and Haldane F D M 2005 *Phys. Rev. Lett.* **95** 136602
[8] Hankiewicz E M, Molenkamp L W, Jungwirth T and Sinova J 2004 *Phys. Rev.* B **70** 241301
[9] Haldane F D M 1988 *Phys. Rev. Lett.* **61** 2015
[10] Kane C L and Mele E J 2005 *Phys. Rev. Lett.* **95** 226801
[11] Altshuler B L 1985 *JETP Lett.* **41** 648

Lee P A and Stone A D 1985 *Phys. Rev. Lett.* **55** 1622
Lee P A, Stone A D and Fukuyama H 1987 *Phys. Rev.* B **35** 1039
[12] Ren W, Qiao Z, Wang J, Sun Q and Guo H 2006 *Phys. Rev. Lett.* **97** 066603
[13] Sheng D N, Sheng L and Weng Z Y 2006 *Phys. Rev.* B **73** 233406
[14] López-Sancho *et al* 1984 *J. Phys. F: Met. Phys.* **14** 1205
López-Sancho *et al* 1985 *J. Phys. F: Met. Phys.* **15** 851